Talwar and Becla, J Material Sci Eng 2016, 5:5
DOI: 10.4172/2169-0022.1000273

Journal of Material Sciences & Engineering

Research Article Open Access

Polarization Dependent Reflectivity and Transmission for $Cd_{1-X}zn_xte$/GaAs (001) Epifilms in the Far-Infrared and Near-Infrared to Ultraviolet Region

Talwar DN[1]* and Becla P[2]

[1]Department of Physics, Indiana University of Pennsylvania, Pennsylvania, USA
[2]Department of Materials Science and Engineering, Massachusetts Institute of Technology, Cambridge, Massachusetts, USA

Abstract

The results of a comprehensive experimental and theoretical study is reported to empathize the optical properties of binary GaAs, ZnTe, CdTe and ternary $Cd_{1-x}Zn_xTe$ (CZT) alloys in the two energy regions: (*i*) far-infrared (FIR), and (*ii*) near-infrared (NIR) to ultraviolet (UV). A high resolution Fourier transform infrared spectrometer is used to assess the FIR response of GaAs, ZnTe, CdTe and CZT alloys in the entire composition $1.0 \geq x \geq 0$ range. Accurate model dielectric functions are established appositely to extort the optical constants of the binary materials. The simulated dielectric functions $\tilde{\varepsilon}(\omega)$ and refractive indices $\tilde{n}(\omega)$ are meticulously appraised in the FIR → NIR → UV energy range by comparing them against the existing spectroscopic FTIR and ellipsometry data. These outcomes are expended eloquently for evaluating the polarization dependent reflectivity $R(\lambda)$ and transmission $T(\lambda)$ spectra of ultrathin CZT/GaAs (001) epifilms. A reasonably accurate assessment of the CZT film thickness by reflectivity study has offered a credible testimony for characterizing any semiconducting epitaxially grown nanostructured materials of technological importance.

Keywords: Fourier transform infrared spectroscopy; Reflectivity; Transmission; Ellipsometry; Dielectric functions; Epilayers

Introduction

The binary cadmium chalcogenides (CdX with X=S, Se, Te) and their ternary ($Cd_{1-x}Y_xX$ with Y=Be, Mg, Zn, and Hg) alloys belong to the group of a II-VI semiconductor family – exhibiting many intriguing properties with a wide-range of applications in photovoltaics, *x*-ray, *γ*-radiation sensors, electro-optical modulators including its usage as a substrate for HgCdTe based infrared (IR) detectors. As compared to the traditional Si and Ge detectors, requiring cryogenic cooling and consuming high power – the II-VI based devices [1-6] are compact, expend less power, operate at room-temperature and display unique features for processing more than one million photons/second/mm^2. In recent years, the growing interest for exploiting $Cd_{1-x}Zn_xTe$ (CZT) epifilms over group-IV semiconductors has been its ability to concoct alloys with accurate control of composition *x* and thickness *d*. The other advantages of utilizing these materials in device engineering include the accessibility of low-cost, large area, and electrically conductive substrates, such as GaAs. For the technological needs, the imperative qualities of CZT comprise of its higher atomic number *Z*, high mass density ρ and large bandgaps E_g [1.45 eV (CdTe), 2.26 eV (ZnTe)] for ensuring enhanced energy resolution and higher detection efficiency. While the key interest in $Cd_{1-x}Zn_xTe$ alloys, and $(CZT)_m$/$(ZnTe)_n$ superlattices (SLs) aspires assessing their electrical and optical characteristics by controlling *x*, *m* and *n* – the film thickness *d* plays an equally important role in regulating the efficiency of electro-optical devices, e.g., an accurate thickness of buffer and epifilm is required for fabricating sensors, detectors, and solar-cells [4-6].

The II-VI based electronics demand [7-10] high-quality crystalline materials with fewer defects. In the as grown CZT alloys, the constraints of phase diagram necessitating higher growth temperatures usually instigate intrinsic defects. In the electronic industry, as the veracity of using semiconductor materials intensifies – so does the compulsion of employing reliable and reproducible methods for appraising their distinctive qualities. In assessing the nature of defects and degree of crystallinity, many experimental techniques have been employed in the past, such as the Fourier transform infrared (FTIR) reflectivity and transmission [9,10], Raman scattering (RS) [8], photoluminescence (PL) [11], synchrotron X-ray diffraction (S-XRD) topography [1-3], and deep level transient spectroscopy (DLTS) [12], etc. In addition, the spectroscopic ellipsometry (SE) is perceived as an equally valuable tool for appraising the optical constants of semiconductor materials and evaluating the epifilm thickness [13].

Despite the extensive technological needs, a limited number of experimental/theoretical studies are carried out on the fundamental properties of CZT alloys and SLs – especially the physics behind those attributes which ascertain their prominence at a practical level. Although, a significant amount of work exists dealing with the growth and electronic characteristics of II-VI materials – the structural, and optical properties of $Cd_{1-x}Zn_xTe$ are either scarcely known [6-8] or ambiguous. In the far-infrared (FIR) region 5 meV ≤ E ≤ 100 meV, while SE is recognized as an efficient method for exploring lattice dynamics and free carrier concentration in semiconductors – it has not yet been applied to study the phonons of CZT alloys. Again, no SE measurements are available for assessing the $Cd_{1-x}Zn_xTe$/GaAs epifilm thickness. Earlier, the vibrational properties of $Cd_{1-x}Zn_xTe$ were acquired by using FTIR [9,10] and RS [8] spectroscopy with a limited alloy composition, *x*. The results when analyzed by a classical method envisioned a "two-phonon-mode" behavior. Recently, we have performed extensive micro-Raman and extended X-ray absorption fine-structure (EXAFS) measurements on the Bridgman-grown $Cd_{1-x}Zn_xTe$ alloyed samples [14,15] in the entire composition range $1.0 \geq x \geq 0.0$ and comprehended their phonon and structural traits. A careful evaluation of the experimental data by an average-t-matrix

***Corresponding author:** Talwar DN, Department of Physics, Indiana University of Pennsylvania, 975 Oakland Avenue, 56 Weyandt Hall, Indiana, Pennsylvania 15705-1087, USA, Tel: 7243572100; E-mail: talwar@iup.edu

Received July 14, 2016; **Accepted** July 27, 2016; **Published** August 06, 2016

Citation: Talwar DN, Becla P (2016) Polarization Dependent Reflectivity and Transmission for $Cd_{1-x}zn_xte$/GaAs (001) Epifilms in the Far-Infrared and Near-Infrared to Ultraviolet Region. J Material Sci Eng 5: 273. doi:10.4172/2169-0022.1000273

Green's function (ATM-GF) approach has authenticated the "two-phonon mode" stance [14]. While the composition-dependent EXAFS data revealed a bimodal distribution of nearest-neighbor bond lengths–theoretical analysis by first-principles bond-orbital model permitted an accurate appraisal of the lattice relaxations around Zn/Cd atoms in CdTe/ZnTe materials. One must note that only limited efforts have been made by SE to uncover the optical properties of CZT alloys in the near-IR (NIR) to ultraviolet (UV) energy range [16-20]. From a theoretical stand point, it has now become possible [14,15] to expend pragmatic model dielectric functions (MDFs) of binary materials to elucidate structural and optical characteristics of semiconducting ternary alloys, and SLs grown on different substrates. Earlier, it was comprehended that only first principles methods could yield material characteristics with accuracies required of the experiments [21]. It is, therefore, quite intriguing to explore electrical and optical properties of novel CZT alloys [22-25] which are playing crucial roles in contriving IR detectors/sensors, photovoltaic-cells, and many other optoelectronic devices [1-6]. The purpose of this paper is to report the results of comprehensive experimental and theoretical investigations to apprehend the structural and optical characteristics of ultrathin (20 nm ≤ d ≤ 1.0 μm) $Cd_{1-x}Zn_xTe$ epifilms prepared on GaAs substrate. Accurate model dielectric functions are established appositely to extort the optical constants of all the involved semiconductor materials. The simulated dielectric functions $\tilde{\varepsilon}(\omega)$ and refractive indices $\tilde{n}(\omega)$ are meticulously appraised in the FIR → NIR → UV energy range by comparing them against the existing spectroscopic FTIR [9] and ellipsometry [20] data. A traditional approach of multilayer optics is used to simulate polarization dependent reflectivity [$R(\lambda)$] and transmission [$T(\lambda)$] spectra for ultrathin $Cd_{1-x}Zn_xTe$/GaAs (001) epifilms of thickness ranging between 22 nm ≤ d ≤ 1 μm. Theoretical results of $R(\lambda)$ and $T(\lambda)$ are compared, discussed and contrasted amongst the available experimental data [22-29] with concluding remarks presented in Section 7. An accurate assessment of film thickness by reflectivity study has offered a credible testimony for characterizing epitaxially grown nanostructured materials of diverse technological importance.

Experimental

$Cd_{1-x}Zn_xTe$ ternary alloys

The $Cd_xZn_{1-x}Te$ ($0 \le x \le 1$) samples used in the FIR (5 meV ≤ E ≤ 100 meV) reflectivity measurements [9] were grown at the Massachusetts Institute of Technology using the Bridgman technique. The CZT ternary alloys were prepared by reacting the 99.9999% pure elemental constituents in the evacuated sealed quartz tubes at ~ 1150°C. The Cd composition values x determined from the mass densities and the precast alloys were re-grown by directional solidification at the rates of 1.2 mm/h in the adiabatic zone of a Bridgman-Stockbarger type furnace with temperature gradient set at about 15°C/cm. The resultant boules cut into 1-2 mm thick slices perpendicular to the growth axis were annealed at 600°C in a Cd-saturated atmosphere for about 5 d to improve the crystalline perfection. Finally, the surfaces of the CZT sample were prepared by lapping, mechanical polishing, and etching in a bromine-methanol solution. The alloy composition x, set by the ratio of constituents before growth was confirmed by the x-ray diffraction and transmission measurements after preparation. All the samples were found to be single-crystal with the zinc-blende structure.

Far-infrared reflectivity

The room temperature FIR reflectance spectra on the $Cd_xZn_{1-x}Te$ ($0 \le x \le 1$) ternary alloy samples were measured at near normal incidence by using a Bruker IFS66 spectrometer with KBr beam-splitter and a deuterated triglycine sulfate (DTGS) detector to achieve a good signal to noise ratio in the energy region 5 meV ≤ E ≤ 100 meV. The details of FIR measurements are described elsewhere [9] where we set the incident angle at about 9°C degrees–a negligible deviation from the near normal incidence. The experimental reflectance spectra was analyzed theoretically by using a classical "Drude-Lorentz" methodology – creating effective MDF's and including contributions from both the lattice phonons as well as free charge carriers.

Theoretical Background

The customary SE parameters Ψ and Δ are related [13] to the ratio ρ of the complex Fresnel reflection coefficients $\tilde{r}^p$ and $\tilde{r}^s$, respectively for the incident light polarized parallel (||) and perpendicular (⊥) to the plane of incidence:

$$\rho \equiv \frac{\tilde{r}^p}{\tilde{r}^s} = \tan\Psi \exp(i\Delta) \tag{1}$$

The SE method is considered quite methodical compared to the reflected intensity measurements – generally performed at a near normal incidence. Again, thickness measurement by in-line SE [13] has played an important role for monitoring the epitaxial film growth processes. For extracting the optical constants and thickness of layer structured materials in the energy range of 0.5 eV to 10 eV, one needs to establish reasonably accurate MDF's to simulate the complex dielectric functions, $\tilde{\varepsilon}(\omega)$ or refractive indices, $\tilde{n}(\omega)$ for both the epifilms and substrates.

In simulating the reflectance and transmission spectra of epifilms, a three phase (Figure 1) model (ambient (air)/film/substrate) [30] is considered to be convincingly adequate. For modeling the optical properties, we have pretended that both the epifilms and substrates form homogenous isotropic materials while the ambient is viewed as non-absorbing. In the framework of classical methodology of multilayer optics, the isotropic $Cd_{1-x}Zn_xTe$ film of thickness d (Figure 1) is described by a material of complex refractive index $\tilde{n}_1$ grown on a thick GaAs substrate of refractive index $\tilde{n}_2$. The incident light of wavelength λ from the ambient of refractive index $\tilde{n}_0$ (≡1) causes many reflections and transmissions at the substrate/film and film/air interface. Due to multiple reflections within the film, the reflected electric fields parallel and perpendicular to the plane of incidence adds up by a geometric series giving an Airy formula for the reflection $\tilde{r}^x$ coefficient ($x \equiv s$-, p- polarization) [14]:

$$\tilde{r}^x = \frac{\tilde{r}^x_{01} + \tilde{r}^x_{12} e^{2i\beta}}{1 + \tilde{r}^x_{01}\tilde{r}^x_{12} e^{2i\beta}} \tag{2}$$

where, $\tilde{r}^x_{01}$, $\tilde{r}^x_{12}$ are the Fresnel coefficients describing the reflection at the respective interfaces between media of refractive indices $\tilde{n}_0$, $\tilde{n}_1$ and among $\tilde{n}_1$, $\tilde{n}_2$. The film thickness d and the angle of incidence

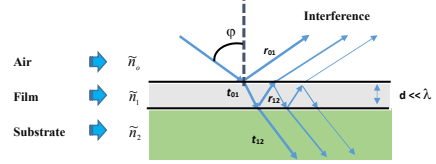

Figure 1: The sketch of a three phase model for calculating reflectivity and transmission spectra of ultrathin $Cd_{1-x}Zn_xTe$/GaAs (001) epifilms.

ϕ are restricted within the phase factor $\beta = 2\pi \frac{d}{\lambda}\sqrt{\tilde{n}_1^2 - \tilde{n}_0^2 \sin^2\phi}$. By using Eq. (2) we have calculated the polarization dependent reflectivity $R^x = |\tilde{r}^x|^2$ spectra for ultrathin $Cd_{1-x}Zn_xTe$ epifilms prepared on GaAs (001) substrate. Similar calculations for the polarization dependent transmission $T^x = |\tilde{t}^x|^2$ are also performed. The results presented are compared and contrasted against the limited experimental data [22-29].

The model dielectric functions

Far-IR to mid-IR energy range: For $Cd_{1-x}Zn_xTe$ ternary alloys, the contribution of polar lattice phonons to the dielectric response $\{\tilde{\varepsilon}_L(\omega)\}$ is evaluated within the reststrahlen band region by exploiting a classical "Drude-Lorentz" model [9]:

$$\tilde{\varepsilon}_L(\omega) = \varepsilon_{\infty x}\left[1 - \frac{\omega_p^2}{\omega(\omega + i\gamma_p)}\right] + \sum_{j=1,2}\frac{S_{jx}\omega_{TOj}^2}{\omega_{TOjx}^2 - \omega^2 - i\Gamma_{jx}\omega} \quad (3)$$

Here, the term $\varepsilon_{\infty x}$ represents the weighted high-frequency dielectric function; ω_{TOjx}- the CdTe-like and ZnTe-like TO-mode frequencies; S_{jx}- the oscillator strengths; Γ_{jx} -the broadening values of TO phonons; ω_p represents the plasma frequency and γ_p its damping constant. The plasma frequency $\omega_p\left(\equiv\sqrt{\frac{4\pi\eta e^2}{m^*\varepsilon_\infty}}\right)$ and $\gamma_p\left(\equiv\frac{e}{m^*\mu}\right)$ of the free carriers (electrons) are assessed from the effective mass m^*, the carrier concentration η, magnitude of the electron charge e and mobility μ. For simulating the reflectance and transmission spectra of $Cd_{1-x}Zn_xTe$/GaAs (001) and/or $(CdTe)_m/(ZnTe)_n$/GaAs (001) SLs, the required $\tilde{\varepsilon}_L(\omega)$ for the substrate (GaAs) is calculated independently. To attain the best-fit parameter values in Eq. (3), we followed an efficient Levenberg-Marquardt algorithm [31] and used the non-linear simulations to minimize the error function Ξ over n data points:

$$\hat{\Xi} = \frac{1}{n}\sum_i^n |\Re_i^{exp} - \Re_i^{cal}|^2 \quad (4)$$

where, $\Re_i^{exp}$, $\Re_i^{cal}$ are the experimental and calculated values, respectively.

Near-IR to UV energy range: In the NIR to UV (0. 5 eV to > 7.0 eV) spectral range, the dielectric behaviors of crystalline materials are strongly allied to their energy-band structures [13]. It has been well established that in semiconductors both direct and indirect band gap transitions near the critical points (CPs) affect optical dispersion relations. In the indirect-band-gap semiconductors, while the transitions take place at energies below the onset of the lowest direct transitions–in the direct-band-gap materials the transitions take part at energies above the onset of the lowest direct transitions [32]. The electronic energy band structures of CdTe, ZnTe and GaAs have been extensively studied both theoretically [33] and experimentally [34-41]. In the experimental studies, several inter-band transitions related to CPs at different parts of the Brillouin zone (BZ) have been identified by exploiting reflectivity [34], SE [13], electro-reflectance [35], thermo-reflectance [36], and wavelength-modulated reflectivity [37] techniques.

In our simulations of the complex dielectric functions $\tilde{\varepsilon}(\omega)$ for the direct bandgap binary compounds CdTe, ZnTe and GaAs, we instigated Adachi's [16,20] optical dispersion mechanisms by exploiting the modified model dielectric functions. Based on the Kramers-Krönig (KK) transformation, this methodology [32] predicts very well the distinct optical features of the perfect materials near CPs in the BZ. In this approach, one anticipates to have three fitting constraints for each CP transitions: the energy, strength and broadening parameter. For instance, the transition energies at CPs near Γ (i.e., at the center of the BZ); Λ or L (in the <111>); and X (in the <100>) points are labeled as E_0, $E_0+\Delta_0$; E_1, $E_1+\Delta_1$; and E_2, respectively [20]. While the E_0, $E_0+\Delta_0$, transitions at Γ point are of the three-dimensional (3D) M_0-type – the E_1, $E_1+\Delta_1$ transitions, take place in the <111> direction near Λ or L points in the BZ, are of 3D M_1-type. Since the M_1-CP longitudinal effective mass is much larger than its transverse counterparts, one can treat 3D-M_1 CPs as two dimensional (2D) minimum M_0 [20]. Again, a pronounced structure in the optical spectra of CdTe and ZnTe near X point in the <100> direction having energy higher than $E_1+\Delta_1$ is labeled as E_2. In general, the E_2 transition does not correspond to a single well-defined CP – it has been characterized by a damped harmonic oscillator.

For calculating the optical constants of ternary $Cd_{1-x}Zn_xTe$ alloys, the CP energies are represented by quadratic expressions involving binary energy values and composition, x while the strength and broadening parameters are assumed varying linearly with x. The relevant expressions of MDFs reported elsewhere [32] for each energy gaps are used in assessing the spectral dependence of various optical constants – linked to the dielectric function $\tilde{\varepsilon}(\omega)$. For instance, the complex refractive index $\tilde{n}(\omega)$ is allied to:

$$\tilde{n}(\omega) = n(\omega) + ik(\omega) = \sqrt{\tilde{\varepsilon}(\omega)} \quad (5)$$

where, the refractive index $n(\omega)$, extinction coefficient $k(\omega)$ and absorption coefficient $\alpha(\omega)$ are expressed as:

$$n(\omega) = \left[\frac{(\varepsilon_1^2 + \varepsilon_2^2)^{1/2} + \varepsilon_1}{2}\right]^{1/2} \quad (6a)$$

$$k(\omega) = \left[\frac{(\varepsilon_1^2 + \varepsilon_2^2)^{1/2} - \varepsilon_1}{2}\right]^{1/2} \quad (6b)$$

$$\alpha(\omega) = \frac{4\pi}{\lambda}k(\omega) \quad (6c)$$

with $\varepsilon_1(\omega) = \mathrm{Re}\,\tilde{\varepsilon}(\omega)$ and $\varepsilon_2(\omega) = \mathrm{Im}\,\tilde{\varepsilon}(\omega)$.

One must note that $\varepsilon_1(\omega)$ describes the refraction of photons at any energy range, while $\varepsilon_2(\omega)$ plays a crucial role near the characteristic resonances where the material absorbs electromagnetic radiation. For instance, in polar semiconductors, the distinct resonances in the FIR energy region arise from the transverse optical (ω_{TO}) vibrational modes. In bulk materials, the optical constants can be appraised by SE [13] and other experiments [34-41] – exploiting specific wavelengths ranging from FIR → NIR → UV. Theoretically, the dielectric functions $\tilde{\varepsilon}(\omega)$ or refractive indices $\tilde{n}(\omega)$ are extorted fitting SE data by expending the well-known KK analysis [13]. However, such a methodology cannot be offered to explicate the optical properties of epilayers prepared on a substrate. Again, from the traditional transmission/reflectance methods [27,28] adopted by others – it is equally impractical acquiring optical parameters of ultrathin films due to small and feeble interference patterns. Here, we have extorted the energy dependent dielectric constants by using accurate MDFs for both the binary GaAs and ternary $Cd_{1-x}Zn_xTe$ alloys and successfully evaluated epifilm thickness by assimilating a procedure outlined.

Numerical Computations and Results

Optical constants in the FIR region

In the photon energy range 100 meV ≥ E ≥ 5 meV, we have

established the MDFs for CdTe, $Cd_{1-x}Zn_xTe$ and GaAs in terms of harmonic oscillators within the classical "Drude-Lorentz" methodology [9]– requiring contributions from the polar lattice phonons and free-charge carriers (Table 1a and 1b). In Figure 2a, we displayed our experimental results of the FIR reflectivity at near normal incidence for GaAs and compared it with the best-fit model calculation (using Eq. (3)). The derived optical parameters n, k and ε_1, ε_2 are included in Figures 2b and 2c, respectively. The perusal of Figure 2b has revealed the long wavelength TO phonon energy near ~34 meV (~ 270 cm^{-1}) at the peak of $\varepsilon_2(\omega)$ while the LO phonon mode (Figure 2c) is perceived near ~37 meV (~ 295 cm^{-1}) at $n = k$ with $\varepsilon_1(\omega) = 0$. For $Cd_{1-x}Zn_xTe$ alloy [9] with $x = 0.2$, the analysis of our FIR reflectivity spectra (Figure 3a) at near normal incidence offered optical parameters (Figures 3b and 3c) in excellent affirmation to the RS results [14] revealing CdTe-like (TO_1, LO_1) and ZnTe-like (TO_2, LO_2) modes. Not only these observations provided strong corroboration to the polarization dependent results (Figure 3d) but are also found consistent with the recent elucidations of the two-phonon-mode behavior predicted by RS and modified random element iso-displacement (MREI) model [8-10]. In the absence of FIR-SE data for $Cd_{1-x}Zn_xTe$ alloys, our simulations of ε_1 and ε_2 agreed fairly well with the experimental data of $Cd_{0.925}Be_{0.075}Se$ [42].

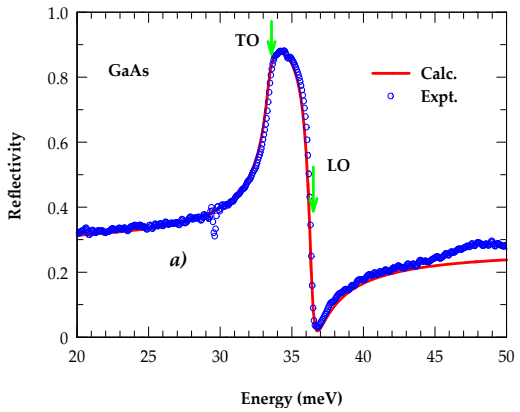

Figure 2a: Comparison of the experimental FIR reflectivity spectra for GaAs represented by blue color open circles (◯) with the best fit simulated reflectivity results shown by red color solid line (—) using a classical Drude-Lorentz model (Eq. 3) with parameter values from Table 1 b) – green colored vertical arrows are used to represent TO and LO modes.

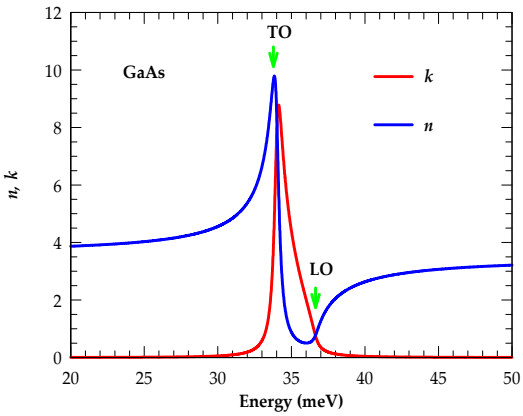

Figure 2b: The simulated results of index of refraction n(ω) and extinction coefficient k(ω).

Optical constants in the NIR-UV region

By exploiting Adachi's formalisms [13,16] and using the modified MDFs, we have numerically simulated ε_1, ε_2, n, k at the photon energy range of 10 eV ≥ E ≥ 0.5 eV for both the binary and ternary alloy semiconductors. Theoretical results of the optical constants shown in

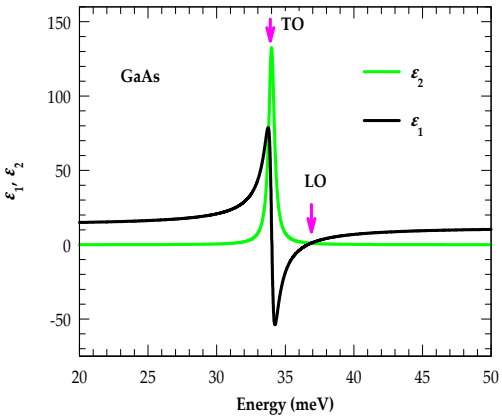

Figure 2c: The real $\varepsilon_1(\omega)$ and imaginary $\varepsilon_2(\omega)$ part of the complex dielectric function $\tilde{\varepsilon}(\omega)$ for GaAs.

(a) $Cd_{1-x}Zn_xTe$[9]300K										
CdTe-like mode				ZnTe-like mode						
x	ε_∞	S_1	ω_{TO1} (cm^{-1})	Γ_1 (cm^{-1})	S_2	ω_{TO2} (cm^{-1})	Γ_2 (cm^{-1})	η 10^{14} cm^{-3}	m*/m	m cm^2/V-s
0.0	8.52	3.7	141.7	8.63				2.06	0.11	138.4
0.1	6.66	3.67	144.8	9.29				3.07	0.11	120.07
0.2	8.17	3.2	145.6	9.28	0.45	171.73	13.10	4.83	0.11	100.0
0.3	7.96	2.90	149.2	12.9	0.64	176.52	11.51	4.35	0.11	90.0
0.4	8.00	2.36	152.2	11.64	1.07	178.62	10.33	6.05	0.12	87.0
0.5	7.81	2.2	152.0	13.72	0.93	182.07	9.83	8.27	0.12	85.0
0.9	7.05	0.15	158.0	15.0	2.33	182.0	7.72	19.12	0.14	61.2
1.0	6.91				3.64	182.5	5.48	22.10	0.15	64.47

(b) GaAs[9] 300K			
ε_∞	S	ω_{TO} (cm_{-1})	Γ (cm_{-1})
11.1	1.95	268.2	2

[a] Ref. [9]

Table 1: Experimental FTIR (300K) data fitted exploiting the dielectric response model. The set of parameters are evaluated by least square fitting procedure *a*) for the ternary $Cd_{1-x}Zn_xTe$ alloys and *b*) for GaAs in the long wavelength limit.

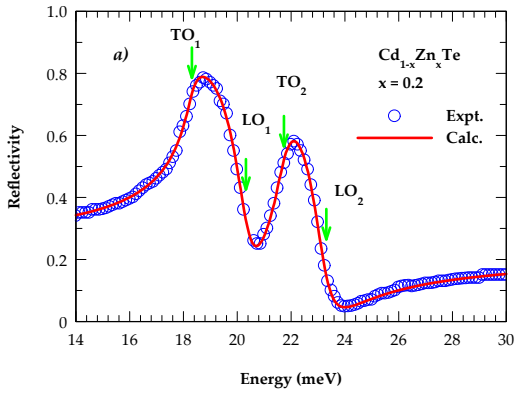

Figure 3a: Comparison of the experimental FIR reflectivity spectra of $Cd_{1-x}Zn_xTe$ (x=0.2) with the best fit calculation from the classical Drude-Lorentz model (Eq. 3) with parameter values from Table 1a.

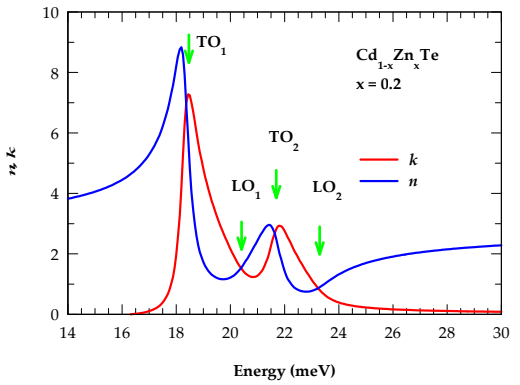

Figure 3b: The simulated results of index of refraction $n(\omega)$, extinction coefficient $k(\omega)$.

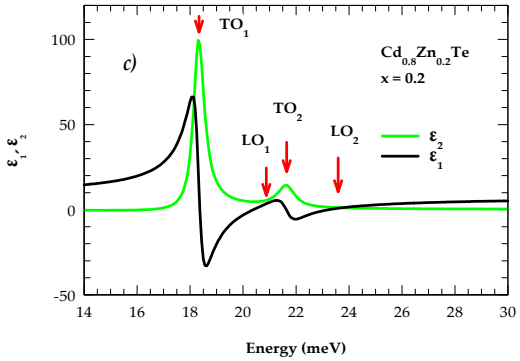

Figure 3c: The real $\varepsilon_1(\omega)$ and imaginary $\varepsilon_2(\omega)$ parts of the complex dielectric function $\tilde{\varepsilon}(\omega)$.

Figures 4a-4e for CdTe, ZnTe and GaAs are compared with the existing SE data [38-40]. Not only, the dispersions of the pseudo-dielectric functions (Figures 4a-4e) concurred well with the experimental data for the binary materials–the results have clearly revealed distinct CP features from the band structures arising from inter-band transitions. In calculating the optical constants for the $Cd_{1-x}Zn_xTe$ ternary alloys with x=0.0, 0.11, 0.64, 0.86 and 1.0 (Figures 5a and 5b), we have evaluated the CP energy parameters from the values of its binary counterparts and used the quadratic expressions involving x, while the energy strength and broadening parameters are obtained deliberating linear dependence articulations on x. Once again, the results (Figures 5a and 5b) of the optical parameters for ternary $Cd_{1-x}Zn_xTe$ alloys are found not only consistent with the limited SE data [16-19] but has also provided clear revelations of the composition dependent CP energy shifts and widths.

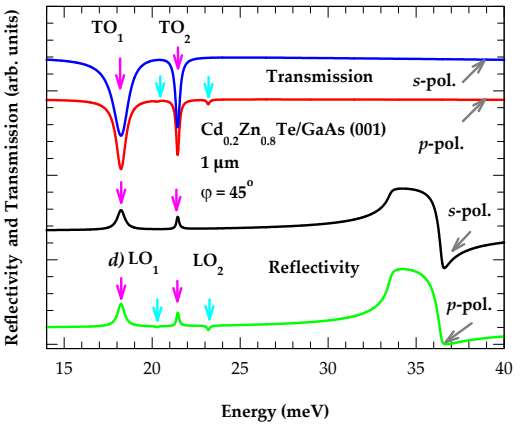

Figure 3d: The polarization dependent transmission (upper panel) and reflectivity spectra (lower panel) for $Cd_{1-x}Zn_xTe$ (x = 0.2) with an incident angle φ = 45°.

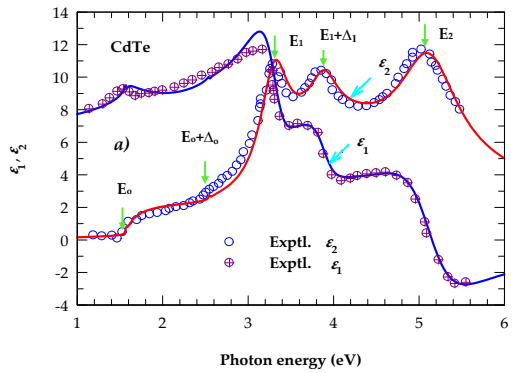

Figure 4a: Comparison of the spectroscopic ellipsometry data for the complex dielectric function $\tilde{\varepsilon}(\omega)$ with the best fit simulated spectra based on a modified MDF for CdTe.

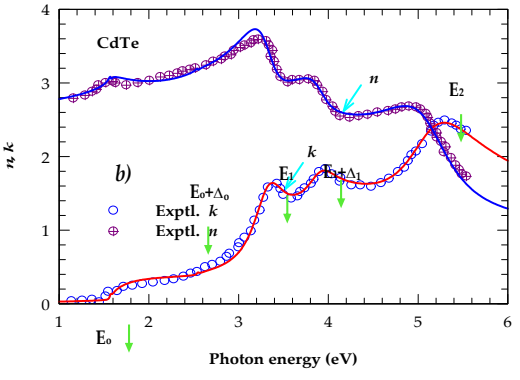

Figure 4b: The comparison of the experimental data with the best fit spectra for the complex refractive index $\tilde{n}(\omega)$ of CdTe.

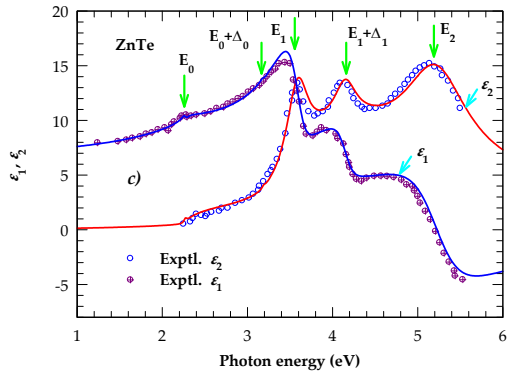

Figure 4c: Similar results [as of *a*)] showing comparison of the experimental complex dielectric function $\tilde{\varepsilon}(\omega)$ with the best fit spectra for ZnTe.

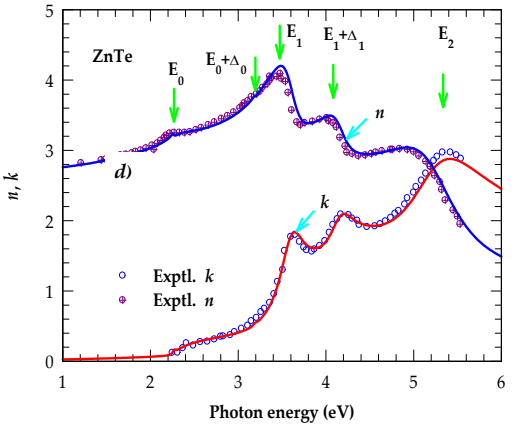

Figure 4d: Similar results [as of *b*)] showing comparison of the experimental complex refractive index $\tilde{n}(\omega)$ with the best fit spectra for ZnTe.

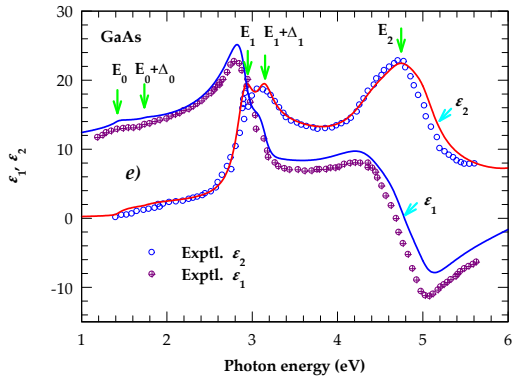

Figure 4e: Similar results [as of *a*)] showing comparison of the experimental complex dielectric function $\tilde{\varepsilon}(\omega)$ with the best fit spectra for GaAs.

Reflectivity and transmission spectra

By incorporating the energy dependent optical constants and following the methodology outlined, we have calculated (Figures 6a-6d) the optical reflectivity [$R(\lambda)$] (blue line) and transmission [$T(\lambda)$] spectra (green line) as a function of photon wavelength λ(~150 - 1800 nm) for several ultrathin $Cd_{1-x}Zn_xTe$ epifilms prepared on n-type GaAs (001). Theoretical results of $R(\lambda)$ appraised at near normal incidence are displayed and compared against the existing experimental data (red squares) for various ultrathin ZnTe/GaAs (001) and $Cd_{0.89}Zn_{0.11}Te$/GaAs (001) epifilms [26] having thicknesses ranging between 22 nm–129 nm. The perusal of Figures 6a-6d clearly revealed that the simulated reflectivity spectra not only concurred well with the experiments – the

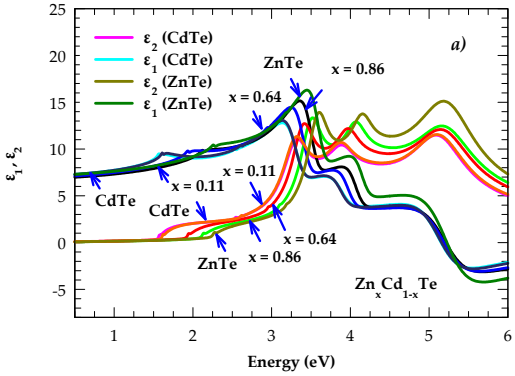

Figure 5a: Calculatedcomplex dielectric function $\tilde{\varepsilon}(\omega)$ spectra based on a modified model dielectric functions for $Cd_{1-x}Zn_xTe$ (x = 0.11, 0.64 and 0.86).

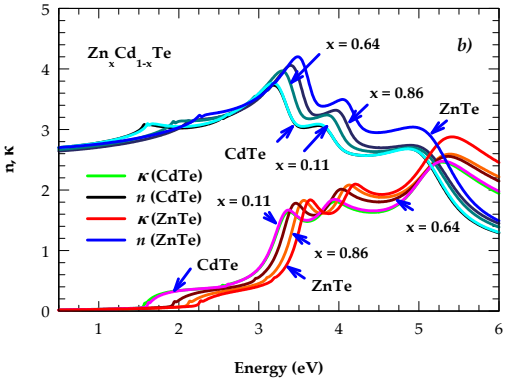

Figure 5b: The calculatedcomplex refractive index $\tilde{n}(\omega)$ spectra based on a modified MDFs for $Cd_{1-x}Zn_xTe$ (x = 0.11, 0.64 and 0.86).

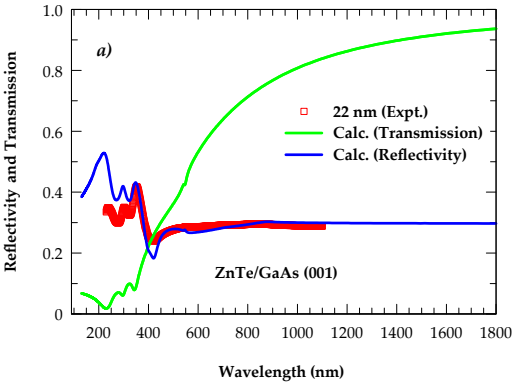

Figure 6a: Comparison of the experimental reflectivity (open red square Ref. [26]) spectra with the simulated reflectivity (solid blue lines) and transmission (solid green lines) spectra for different $Cd_{1-x}Zn_xTe$/GaAs (001) epifilms: for x=1 and d=22 nm.

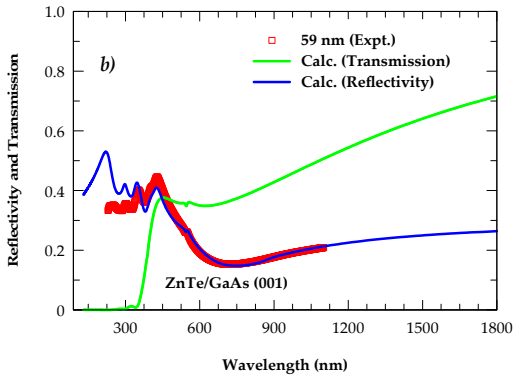

Figure 6b: Comparison of the experimental reflectivity (open red square Ref. [26]) spectra with the simulated reflectivity (solid blue lines) and transmission (solid green lines) spectra for different $Cd_{1-x}Zn_xTe$/GaAs (001) epifilms: for x=1 and d=59 nm.

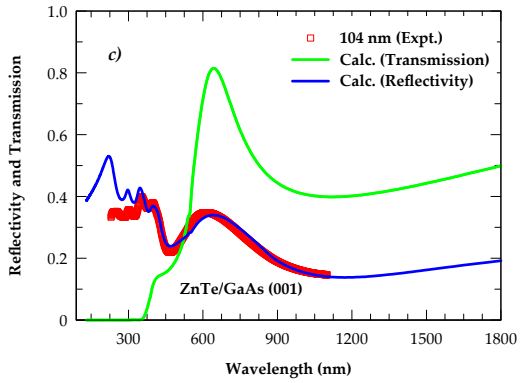

Figure 6c: Comparison of the experimental reflectivity (open red square Ref. [26]) spectra with the simulated reflectivity (solid blue lines) and transmission (solid green lines) spectra for different $Cd_{1-x}Zn_xTe$/GaAs (001) epifilms: for x=1 and d=104 nm.

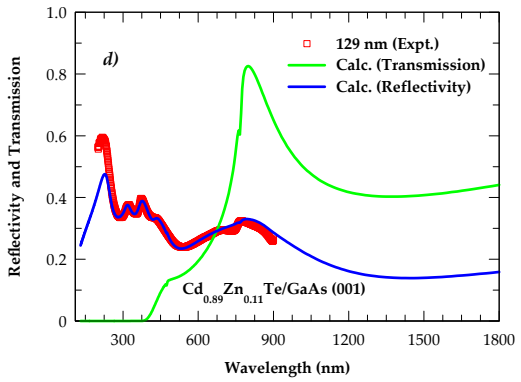

Figure 6d: Comparison of the experimental reflectivity (open red square Ref. [26]) spectra with the simulated reflectivity (solid blue lines) and transmission (solid green lines) spectra for different $Cd_{1-x}Zn_xTe$/GaAs (001) epifilms: for x=0.11 and d=129 nm.

theoretical results have certainly encapsulated all the major observed features. One must note that as the ZnTe ($Cd_{1-x}Zn_xTe$)/GaAs (001) epifilms are too lean, the simulated (Figures 6a-6d) reflectivity [$R(\lambda)$] and transmission [$T(\lambda)$] spectra have divulged no interference fringes in the transparent photon energy region – except that they disclosed the broad intensity modulations. Moreover, for all the material samples studied here – the film thicknesses d assessed by reflectivity studies have concurred copiously with the apparent values appraised from the high resolution X-ray diffraction (HR-XRD) $\omega/2\theta$ scans and other measurements [41].

Thickness dependence: In Figures 7a and 7b, we have displayed the results of our model calculations for the optical reflectivity and transmission spectra of ZnTe/GaAs (001) as a function of λ (100 - 2500 nm) for film thicknesses d varied between 100 nm to 1000 nm. The reflectivity $R(\lambda)$ and transmission $T(\lambda)$ spectra have clearly revealed interference fringes in the highly transparent photon energy region (λ>548 nm). As expected for thicker films – we perceived emergence of fringes when the conditions of constructive and destructive interferences are met between the light waves reflected off the top and bottom of the film – causing maxima and minima, respectively. From the calculated results of transmission $T(\lambda)$ spectra for ZnTe/GaAs films, we also noticed that with the increase of film thickness from 100 nm to 1000 nm, the transmittance (Figure 7b) decreased – eliciting a sharp absorption edge near λ ≡ 548 nm. For ZnTe films with thickness d>400 nm, our assessed optical band gap E_g (≡ 2.26 eV) from the absorption band edge concurred very well with the PL measurement of E_g for the bulk material. In thinner films (d<400 nm) we noticed the absorption band edge divulging a slight blue shift i.e., veering towards the lower λ – possibly prompting slightly larger optical band gaps. This

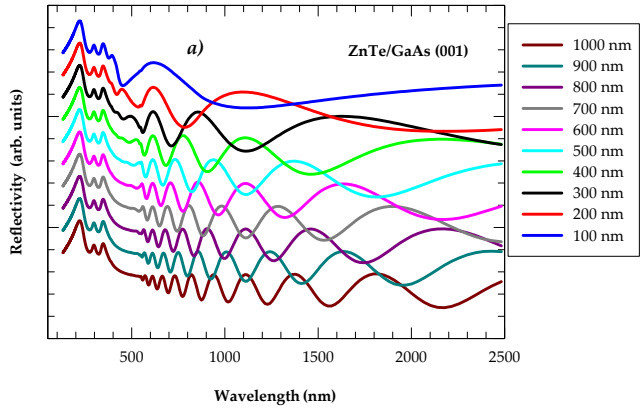

Figure 7a: Thickness dependent reflectivity for ZnTe/GaAs (001) epifilms with d ranging from 100 nm-1000 nm.

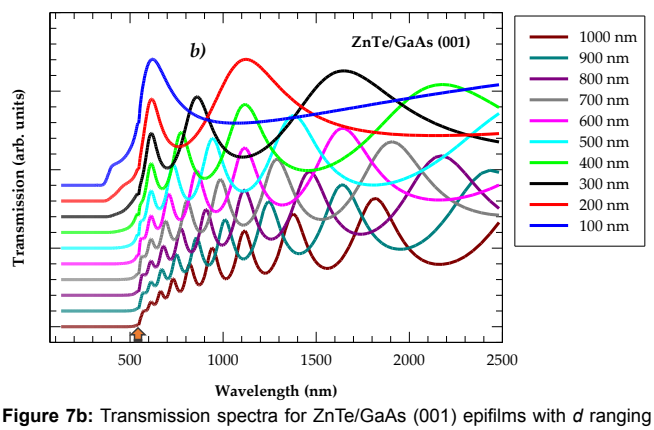

Figure 7b: Transmission spectra for ZnTe/GaAs (001) epifilms with d ranging from 100 nm-1000 nm.

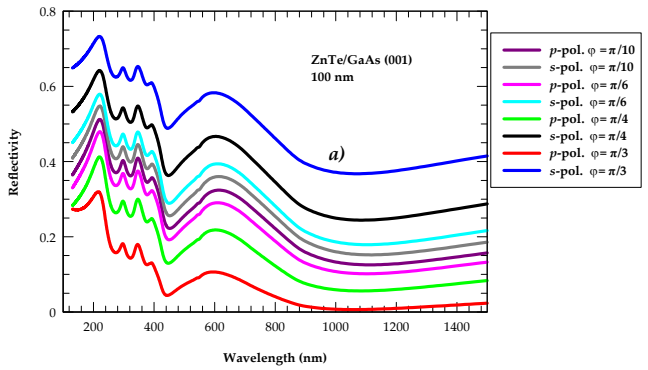

Figure 8a: Polarization dependentreflectivity for ZnTe/GaAs (001) epifilm of thickness 100 nm for incident angle φ ranging from π/10-π/3.

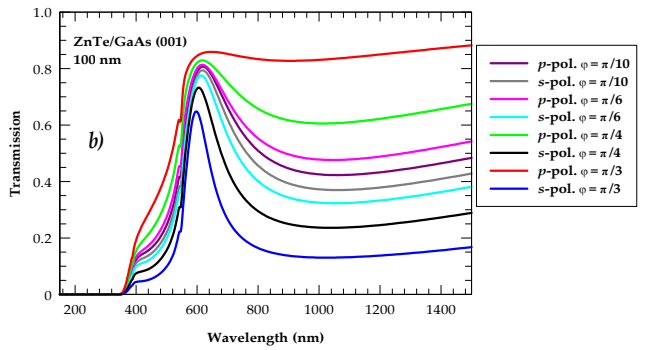

Figure 8b: Transmission spectra for ZnTe/GaAs (001) epifilm of thickness 100 nm for incident angle φ ranging from π/10-π/3.

manifestation in ultrathin ZnTe/GaAs films while not clearly implicit has been recognized, however, in a few recent experiments [26,27] and attributed to the probable misfit strain between the films and substrate.

Polarization Dependence: In Figures 8a and 8b, we have displayed our simulated results of the *s*- and *p*- polarized reflectance $[R^s(\lambda), R^p(\lambda)]$ and transmission $[T^s(\lambda), T^p(\lambda)]$ spectra for a 100 nm thick ZnTe/GaAs (001) epifilm by varying the angle of incidence ϕ from π/10 to π/3 (or from 18° to 60°). The reflectance and transmission spectra for λ between 100-1500 nm in the two polarization states have revealed the typical dispersion features. Our calculations (Figure 8a) have divulged that the *s*-polarized reflectivity $R^s(\lambda)$ increases as the angle of incidence increases from 18 to 60° while the *p*-polarized reflectivity $R^p(\lambda)$ decreases with the increase of incidence angle. On the other hand, the results of *p*-polarized transmission $T^p(\lambda)$ showed (Figure 8a) higher values at larger ϕ as compared to the *s*-polarized transmission $T^s(\lambda)$ spectra. Moreover, the $T^p(\lambda)$ results at 60° have indicated that the ZnTe film is more transparent (~85% in the visible to NIR region) than for the $T^s(\lambda)$ state. This outcome is further verified by the fact that the simulated *s*-polarized reflectivity $R^s(\lambda)$ is larger (Figure 8a) than the *p*-polarized reflectivity $R^p(\lambda)$.

Summary and Conclusions

In summary, we have reported the results of a comprehensive experimental and theoretical study for understanding the optical properties of ZnTe ($Cd_{1-x}Zn_xTe$) and GaAs in a wide spectral range covering the FIR (5 meV ≤ E ≤ 100 meV) and NIR to UV (0.75 eV ≤ E ≤ 10 eV) energy regions. By exploiting a Bruker IFS66 spectrometer, we have measured the FIR response for GaAs, ZnTe, CdTe and $Cd_{1-x}Zn_xTe$ alloys ($1.0 \geq x \geq 0$). Different model dielectric functions are established for extracting the dielectric functions $\tilde{\varepsilon}(\omega)$ of the binary and ternary materials in the two energy regions. In the FIR spectral range, the necessary MDFs are ascertained within the classical Drude-Lorentz [9] methodology by assimilating contributions from both the lattice phonons and free-charge carriers. In the NIR to UV energy region, we have instigated Adachi's [16,20] optical dispersion mechanisms and extorted $\tilde{\varepsilon}(\omega)$ or $\tilde{n}(\omega)$ by exploiting the modified [32] model dielectric functions. The simulated energy dependent optical constants for the binary and ternary alloys compared favorably well with the existing FIR-SE and other experimental [22-29] data. These results are proven valuable for accurately assessing the film thickness *d* from the polarization dependent reflectivity *R*(λ) and transmission *T*(λ) spectra of ultrathin $Cd_{1-x}Zn_xTe$/GaAs (001) epifilms. Clearly, the outcome of this methodology has offered a credible testimony for characterizing any semiconducting epitaxially grown nanostructured films of technological importance.

Acknowledgements

One of the authors (DNT) wishes to thank Dr. Deanne Snavely, Dean, College of Natural Science and Mathematics for the travel support and for an Innovation Grant that he received from School of Graduate Studies at Indiana University of Pennsylvania, Indiana, PA that made this collaborative research possible. The experimental results on the FIR measurements presented in details elsewhere were provided by Professor T. R. Yong (National Taiwan Normal University, Taipei).

References

1. Lohstroh A, Della Rocca I, Parsons S, Langley A, Shenton-Taylor C, et al. (2015) Cadmium zinc telluride based infrared interferometry for X-ray detection. Appl Phys Lett 106: 063507-063510.
2. Franc J, Dědič V, Rejhon M, Zázvorka J, Praus P, et al. (2015) Control of electric field in CdZnTe radiation detectors by above-bandgap light. J App Phys 117: 165702-165707.
3. Gan B, Wei T, Gao W, Zeng H, Hu Y (2013) Design of a low-noise front-end readout circuit for CdZnTe Detectors. Journal of Signal and Information Processing 4: 123-128.
4. Rodrigues BHG, Grindlay JE, Allen B, Hong J, Barthelmy S, et al. (2013) The high resolution X-Ray imaging detector planes for the MIRAX mission.
5. Bolotnikov AE, Babalola S, Camarda GS, Cui Y, Egarievwe SU, et al. (2010) Te inclusions in CZT detectors: New method for correcting their adverse effects. IEEE Trans Nucl Sci 57: 910-919.
6. Cai L, Meng LJ (2013) Hybrid pixel-waveform CdTe/CZT detector for use in an ultrahigh resolution MRI compatible SPECT system. Nucl Instr and Methods in Physics Research A 702: 101-103.
7. Hawkins SA, Aleman EV, Duff MC, Hunter DB, Burger A, et al. (2008) Light-induced tellurium enrichment on CdZnTe crystal surfaces detected by raman spectroscopy. J Electron Mater 37: 1438-1443.
8. Olego DJ, Raccah PM, Faurie JP (1986) Compositional dependence of the Raman frequencies and line shapes of Cd1−x ZnxTe determined with films grown by molecular-beam epitaxy. Phys Rev B 33: 3819-3824.
9. Talwar DN, Yang TR, Feng ZC, Becla P(2011) Infrared reflectance and transmission spectra in II-VI alloys and superlattices. Phys Rev B 84: 174203-174211.
10. Granger R, Marqueton Y, Triboulet R (1993) Optical phonons in bulk Cd1-XZnxTe mixed crystals in the whole composition range. J de Phys 3: 135-141.
11. Teng J, Sang W, Li G, Shi Z, Min J, et al. (2008) Influence of In dopant on PL Spectra of CdZnTe. Crystals J Korean Phys Soc 53: 146-149.
12. Gul R, Keeter K, Rodriguez R, Bolotnikov AE, Hossain A, et al. (2012) Point Defects in Pb-, Bi-, and In-Doped CdZnTe Detectors: Deep-Level Transient Spectroscopy (DLTS) Measurements. J Elect Mater 41: 488-493.
13. Fujiwara H (2007) Spectroscopic ellipsometry: principles and applications. John Wiley, USA.

14. Talwar DN, Feng ZC, Lee JF, Becla P (2013) Structural and dynamical properties of Bridgman-grown CdSexTe1−x (0<x _0.35) ternary alloys. Phys Rev B 87: 165208-165212.

15. Talwar DN, Becla P (2016) Infrared and Raman characteristics of bulk $Cd_{1-x}Mn_xTe$ and (MnTe)m/(CdTe)n short periodsuperlattices. Mat Letts 175: 279-283.

16. Adachi S, Kimura T (1993) Synthesis of self-organized TiO_2 nanotube arrays: Microstructural, stereoscopic, and topographic studies. J Appl Phys 32: 3496-3501.

17. Yao HW, Erickson JC, Barber HB, James RB, Hermon H (1999) Optical Properties of Cd0.9Zn0.1Te studied by variable angle spectroscopic ellipsometry between 0.75 and 6.24 Ev. J Electron Mat 28: 760-765.

18. Daraselia M, Brill G, Garland JW, Nathan V, Sivananthan S (2000) In-situ control of temperature and alloy composition of Cd1-xZnxTe grown by molecular beam epitaxy. J Electron Mat 29: 742-745.

19. Sridharan M, Narayandass SAK, Mangalaraj D, Lee HC (2002) Optical constants of vacuum-evaporated Cd0.96Zn0.04Te thin films measured by spectroscopic ellipsometry. J Mat Sci: Mat Electron 13: 471-476.

20. Adachi S (2005) Properties of Group-IV, III-V and II-VI Semiconductors. John Wiley, USA.

21. Xu M, Li YF, Yao B, Ding Z, Yang G (2014) Structural, electronic and optical properties of $Cd_xZn_{1-x}S$ alloys from first-principles calculations. Phys Lett A 378: 3382-3388.

22. Polizzi E (2009) Density-matrix-based algorithm for solving eigenvalue problems. Phys Rev B 79: 115112.

23. Gygi F (2006) Large-scale first-principles molecular dynamics: moving from terascale to petascale computing. J Phys: Conf Ser 46: 268-277.

24. Windus TL, Bylaska EJ, Tsemekhman K, Andzelm J, Govind N (2009) Computational Nanoscience with NWChem. J Comp Theor Nanosci 6: 1297-1304.

25. Sridharan MG, Mekaladevi M, Rodriguez-Viejo J, Narayandass SK, Mangalraj D, et al. (2004) Spectroscopic ellipsometry studies on polycrystalline $Cd_{0.9}Zn_{0.1}Te$ thin films. Phys Stat Sol 201: 782-790.

26. Larramendi EM, Purón F, Melo O (2002) Thickness measurement and optical properties of Cd1-xZnxTe. Semicond Sci Technol 17: 8-12.

27. Salem AM, Dahy TM, El-Gendy YA (2008) Thickness dependence of optical parameters for ZnTe thin films deposited by electron beam gun evaporation technique. Physica B: Physics of Condensed Matter 403: 3027-3033.

28. Shaaban ER, Ahmad M, Abdel Wahab EA, Shokry Hassan H, Aboraia AM (2013) Structural and optical properties of varies thickness of ZnTe nanoparticle. Proc of Basic and Appl Sci 1: 244-257.

29. Khoshman JM (2005) Spectroscopic ellipsometry characterization of single and multilayer aluminum nitride/indium nitride thin film systems. Dissertation Abstracts International 66: 267.

30. Franta OD (2000) Ellipsometry of thin film systems. Progress in Optics 41: 181-282.

31. Levenberg K (1944) A method for the solution of certain non-linear problems in least square. The Quarterly of Applied Mathematics 2: 164-168.

32. Talwar DN (2009) Novel Dilute III-V-Ns from physics to Applications.

33. Chelikowsky JR, Cohen ML (1976) Nonlocal pseudopotential calculations for the electronic structure of eleven diamond and zinc-blende semiconductors. Phys Rev B 14: 556-566.

34. Guo Q, Ikejira M, Nishio M, Ogawa H (1996) Optical properties of zinc telluride in vacuum ultraviolet region. Solid Stat Commun 100: 813-815.

35. Yasuda K, Kojima K, Mori K, Kubota Y, Nimura T, et al. (1998) Electrical and optical properties of iodine doped CdZnTe layers grown by metalorganic vapor phase epitaxy. J Electron Mater 27: 527-531.

36. Cardona M, Shaklee KL, Pollak FH (1967) Electroreflectance at a semiconductor- electrolyte interface. Phys Rev154: 696-720.

37. Guizzetti G, Nosenzo L, Reguzzoni E, Samoggia G (1974) Thermoreflectance spectra of diamond and zinc-blende semiconductors in the vacuum-ultraviolet region. Phys Rev B 9: 640-647.

38. Aspnes DE, Studna AA (1983) Dielectric functions and optical parameters of Si, Ge, GaP, GaAs, GaSb, InP, InAs, and InSb from 1.5 to 6.0 Ev. Phys Rev B 27: 985-1009.

39. Viña L, Umbach C, Cardona M, Vodopyanov L (1984) Ellipsometric studies of electronic interband transitions in $Cd_xHg_{1-x}Te$. Phys Rev B 29: 6752-6760.

40. Palik ED (1991) Handbook of Optical Constants of Solids. Academic, New York.

41. Hernández LC (2003) Growth of ZnTe Semiconductor Thin films onto GaAs and Si Substrates by Isotherm closed space sublimation.

42. Wronkowska AA, Wronkowski A, Firszt A, Legowski S (2006) Investigation of II-VI alloy lattice dynamics by IR spectroscopic ellipsometry. Cryst Res Technol 41: 580-587.